Journal of Volcanology and Geothermal Research 249 (2013) 12–24

Contents lists available at SciVerse ScienceDirect

Journal of Volcanology and Geothermal Research

journal homepage: www.elsevier.com/locate/jvolgeores

Underwater acoustic records from the March 2009 eruption of Hunga Ha'apai-Hunga Tonga volcano in the Kingdom of Tonga

DelWayne R. Bohnenstiehl [a,*], Robert P. Dziak [b], Haru Matsumoto [b], T.-K. Andy Lau [b]

[a] Department of Marine, Earth and Atmospheric Sciences, North Carolina State University, Raleigh NC 27695, USA
[b] Oregon State University and the National Oceanic and Atmospheric Administration, Hatfield Marine Science Center, Newport OR 97365, USA

ARTICLE INFO

Article history:
Received 25 June 2012
Accepted 20 August 2012
Available online 28 August 2012

Keywords:
Hunga Ha'apai-Hunga Tonga Volcano
Surtseyan eruption
Acoustics
Hydrophone monitoring
Arc volcanism

ABSTRACT

A network of autonomous underwater hydrophones is used to monitor acoustic activity associated with Hunga Ha'apai-Hunga Tonga volcano during a period of 15 months. The data provide a continuous record spanning a surtseyan eruption (VEI 2) in March of 2009, which input ~10^{13} J of acoustic energy into the ocean soundscape. In the months before the eruption, the volcano can be identified as an intermittent source of ambient noise. The period of seismic unrest that precedes the eruption begins at 15:11 UTC on 16 March (04:11 LT on 17 March), approximately 7 h before the first satellite confirmation of eruptive activity and 14 h before the first eyewitness reports. The initial seismic activity, which includes a single 4.8 m_b event at 15:25, evolves as a typical foreshock–mainshock–aftershock sequence. By 15:38, however, the rate of small earthquakes begins to increase, marking the onset of the seismic swarm. The period of highest-amplitude acoustic energy release between 16:40 and ~17:10 is interpreted to mark the opening of the volcanic conduit. By 19:00 on 16 March, the acoustic signature of the volcano is marked by a continuous wide-band (1–20 Hz) noise and a set of transient very-broadband (1–125 Hz) explosion signals. This activity is characteristic of the main surtseyan phase of the eruption. Both the intensity of explosions and the amplitude of the lower frequency wide-band noise decay through time, and eruptive activity likely ends at ~09:00 on 19 March, ~2.7 days after the initiation of seismic activity. At this time the continuous low frequency noise decays to near background levels and signal coherence drops suddenly. Low-level acoustic unrest persists through June of 2009, after which the volcano becomes acoustically dormant during the remaining ten months of monitoring. The analysis of volcano-acoustic signals associated with Hunga Ha'apai-Hunga Tonga volcano highlights the potential role of regional hydroacoustic monitoring in assessing volcanic hazards in arc settings.

1. Introduction

The Tofua volcanic arc is formed by the subduction of the Pacific Plate beneath the Tongan Plate of the extensional Lau Basin. The present-day plate tectonic configuration was initiated following the start of back arc spreading at 5–6 Ma (e.g., Parson and Hawkins, 1994; Parson and Wright, 1996; Taylor et al., 1996). At this time, rifting of the Lau Basin dissected the ancient arc system, forming the Lau and Tonga Ridges that mark the western and eastern boundaries of the basin, respectively. The active volcanic cones of the modern arc are built primarily along the western edge of the relict Tonga Ridge. Those volcanoes that immerge above sea level form young islands within the Tongan chain (Fig. 1).

The uninhabited islands of Hunga Ha'apai and Hunga Tonga mark the western and northern subaerial rim of one such volcanic cone (Fig. 2). The islands are constructed from andesitic lava flows and alternating beds of scoria, lapilli and ash (Bryan et al., 1972). These layers dip gently away from the center of the cone, which is marked by a rocky shoal located ~2 km southeast of Hunga Ha'apai and ~3 km to the south of Hunga Tonga (Fig. 2) (Bryan et al., 1972). During inter-eruptive periods the islands become vegetated and serve as seabird breeding-grounds. Visitors include eco-tourists and sport fishermen. The closest population center is the Tongan capital city of Nuku'afola located 60 km to the south–southeast on Tongatapu Island.

Historical eruptions of the Hunga Ha'apai-Hunga Tonga volcano occurred in 1912, 1937 and 1988 (Siebert et al., 2010). All three are reported to have been centered in the vicinity of the rocky shoal, with aerial observations during the 1988 eruption showing three separate vents aligned in a southwest trend and extending 100–200 m in length (Taylor, 2010). These historical eruptions lasted only a few days and sparse observations indicate volcanic explosivity indexes of VEI 2 for the 1912 and 1937 activity and VEI 0 for the 1988 eruption (Siebert et al., 2010). No new land was produced as a result of these historical eruptions (Siebert et al., 2010; Taylor, 2010).

The volcano erupted most recently in March of 2009, with the first reports of activity coming from commercial airline pilots and passengers at ~05:05 UTC on 17 March (18:05 LT) (Smithsonian Institution, 2009; Taylor, 2010; Vaughan and Webley, 2010). Spectacular images and

* Corresponding author. Tel.: +1 919 515 7449.
E-mail address: drbohnen@ncsu.edu (D.R. Bohnenstiehl).

0377-0273/$ – see front matter © 2012 Elsevier B.V. All rights reserved.
http://dx.doi.org/10.1016/j.jvolgeores.2012.08.014

videos obtained by amateur photographers spurred both regional and global media attention. Although sparse in their temporal sampling, these reports are the primary record of ground-based observations during the episode. Passengers on small boats that approached the islands during the eruption reported two active area of venting, one along the northwestern coastline of Hunga-Ha'apai and the other approximately 100 m south of the island (Smithsonian Institution, 2009; Taylor, 2010) (Fig. 2). The interaction of rising magma with seawater produced a surtseyan eruption style, characterized by series of violent explosions. The largest of these events sent ash and steam to an altitude of 4–7.6 km (15,000–25,000 ft), making the plumes visible from Tongatapu Island and posing a hazard to regional air traffic (Vaughan and Webley, 2010).

During the time period spanning the eruption, Vaughan and Webley (2010) have analyzed data acquired by the satellite-based ASTER and MODIS imaging systems. Available cloud-free scenes constrain the onset of eruptive activity to have occurred between 12:50 and 22:10 UTC on 16 March (01:50 to 11:10 LT on 17 March). The data also indicate that the main phase of eruptive activity lasted only 3–5 days, with continued steam venting occurring for weeks afterwards. Using a time series of images, Vaughan and Webley (2010) show that the land area of Hunga Ha'apai tripled during the eruption, before eroding to roughly twice its original size within six months of the eruption (Fig. 2). Incorporating these land area changes and the area of rafted pumice fields, they report the total volume of eruptive material to be ~0.0176 km^3. Based on the eruptive volume, height of the eruptive column and duration of activity, the eruption is classified as a VEI 2 event (Siebert et al., 2010; Vaughan and Webley, 2010).

This article examines the record of eruptive activity, as monitored by an array of sound-channel moored hydrophones deployed at ranges of approximaely100–500 km from Hunga Ha'apai. While both ship- and satellite-based observations are intermittent, the hydrophone records provide a continuous acoustic time series during a period of 15 months spanning the eruption. The focus of this paper is on documenting the timing, style and underwater acoustic signature of the eruption and its associated seismic activity.

2. Lau hydrophone array

2.1. Overview of instrumentation

During the period of 20 January 2009–15 April 2010, an array of moored hydrophones was deployed within the Lau Basin between 15–23° S and 173–178° W. At the time of the March 2009 eruption of Hunga Ha'apai-Hunga Tonga, the array consisted of five single element stations (M1, M4, M5, M6, M10) and a sixth that hosted a short baseline horizontal array of four sensors deployed in a diamond-shaped configuration (M3, Fig. 1). Each sensor package consisted of a single omni-directional ceramic hydrophone mounted on a titanium pressure case containing a filter/pre-amplifier stage, data logging computer, hard drives and alkaline battery pack (Fox et al., 2001). To take advantage of the efficient propagation of sound in the deep ocean, these recorders were moored by a float near the axis of the sound channel (1000 ± 50 m), where they continuously sampled the ambient sound field at a rate of 250 Hz.

The absolute timing for each instrument was maintained autonomously using a microprocessor controlled temperature-correcting crystal oscillator (MCXO) manufactured by the Q-tech Corporation, models QT2001 (single-element stations) and QT2010 (M3). Each clock was synced with a GPS time before and after deployment. Measured absolute drift rates averaged 1 s/yr for the QT2001clocks; whereas, the QT2010 clocks used for the M3-array drifted only 0.09–0.42 s/yr. The Q-tech clocks' 1-pulse-per-second (1PPS) signals were logged and post-processed for more precise timekeeping, and clock drifts were corrected linearly for each instrument.

Acoustic pressures are measured by removing the frequency-dependent instrument response, and are expressed in units of μPa (10^{-6} Pa) or decibels relative to a reference pressure of 1 μPa. This is the standard reference pressure for underwater acoustics. Readers more familiar atmospheric acoustic measurements can make an approximate conversion to equivalent atmospheric decibel levels by subtracting 63 dB from the values reported.

2.2. Quad-array processing and calibration

The quad-array (M3) is used to estimate the back azimuth of incoming acoustic energy using a plane wave fitting routine (e.g., Del Pezzo and Giudicepietro, 2002; Chapp et al., 2005). The travel time differences between hydrophone pairs (t_{ij}) are estimated from the cross correlation of their low-frequency (2–20 Hz) band passed waveforms. This analysis band exhibits the highest signal-to-noise ratio for Tertiary (T-) wave arrivals sourced from shallow submarine earthquakes (e.g., de Groot-Hedlin and Orcutt, 2001). Given the separation between sensors (1.6–2.8 km), a window length of 5 s is used in all calculations. The horizontal slowness is found by solving the system of equations $\Delta p = t$, where Δ represents a two-column matrix containing the offsets in the x- and y-direction between sensor pairs, t is a column vector of the corresponding time delays, and the vector p represents the two component (p_x, p_y) horizontal slowness. The velocity (v) and azimuth (az) are given as $v = 1/|p|$ and $az = \tan^{-1}(p_x/p_y)$. Reported back-azimuths are filtered for data quality based on the correlation coefficient (cc) between stations pairs, the closure value estimated by summing the lags, $cl = t_{12} + t_{23} + t_{34} + t_{41}$, which should be near zero, and the velocity (v) returned by the inversion, which is expected to be ~1485 m/s for acoustic waves traveling within the low-latitude sound channel.

The resolution and accuracy of the azimuth calculation is verified by using a series of seismic airgun shots produced using the R/V Marcus G. Langseth between 27 January and 24 February 2009 (Dunn and Martinez, 2010; Schiep, 2012). The survey deployed thousands of acoustic sources along the Eastern Lau Spreading Center (ELSC) at ranges of between 30 and 100 km from the M3 array and at back azimuths between 80° and 135°, spanning the ~95° path to Hunga Ha'apai (Fig. 1).

Fig. 3 shows a histogram of the angular difference (°) between the azimuths returned by the inversion and true azimuth estimated from the shot meta-data. Cross-correlations are derived using a 2–20 Hz band-passed signal of 5 s duration capturing the initial arrival of the water-borne phase at the hydrophone. To provide an estimate the azimuthal accuracy as a function of the data quality, the results are filtered based on the returned cc, v and cl values. Coherent arrivals having $cc > 0.6$, $v = 1485 \pm 50$ m/s and $|cl| < 32$ ms (Quality A) show a normal distribution with a mean offset of 0.23° counter clockwise and 0.31° standard deviation. Relaxing these criteria to $cc > 0.5$, $v = 1485 \pm 100$ m/s and $|cl| < 64$ ms (Quality B), the estimated azimuths have a mean offset of 0.25° counter clockwise and 0.57° standard deviation. For arrivals with $cc > 0.4$°, $v = 1485 \pm 150$ m/s and $|cl| < 96$ ms (Quality C), the mean angular offset is 0.30° and one standard deviation uncertainty rises to 0.93°. For all arrivals having $cc > 0.3$, $v = 1485 \pm 200$ m/s and $|cl| < 128$ ms (Quality D), the mean angular offset is 0.25° and one standard deviation uncertainty rises to 1.17°.

These errors may represent uncertainty in transponder-determined positions of the mooring anchors, drift of the hydrophones about their watch circles in response to currents, or non-linear drift among the four autonomous clocks. It also should be noted that airgun sources deployed near the sea surface propagate dominantly via sea bottom reflection (Schiep, 2012), likely degrading their coherence; whereas, volcano-acoustic sources positioned at greater depths may couple directly into the sound channel. Nonetheless, these calibration results show that the method provides sufficient accuracy associate arrivals with the Hunga Ha'apai-Hunga Tonga volcanic edifice. The measured angular resolution and accuracy of the M3-array are consistent with published values for equivalent three-element arrays deployed with a similar aperture as

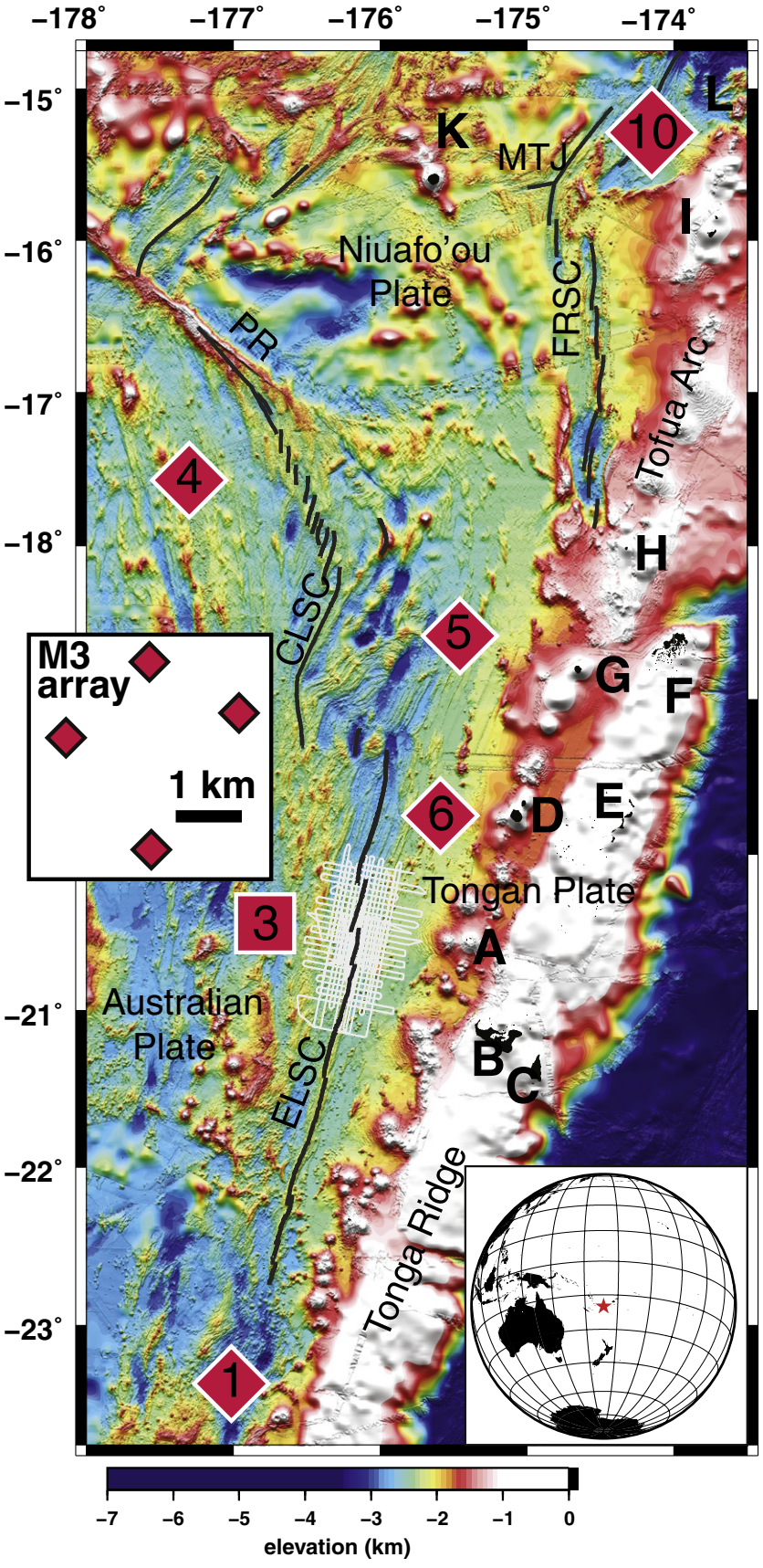
–178°
–177°
–176°
–175°
–174°
–15°
–16°
–17°
–18°
–21°
–22°
–23°
K
MTJ
10
L
I
H
G
F
D
E
A
B
C
Niuafo'ou Plate
PR
FRSC
Tofua Arc
CLSC
ELSC
Tonga Ridge
Tongan Plate
Australian Plate
4
5
6
3
1
M3 array
1 km
–7
–6
–5
–4
–3
–2
–1
0
elevation (km)

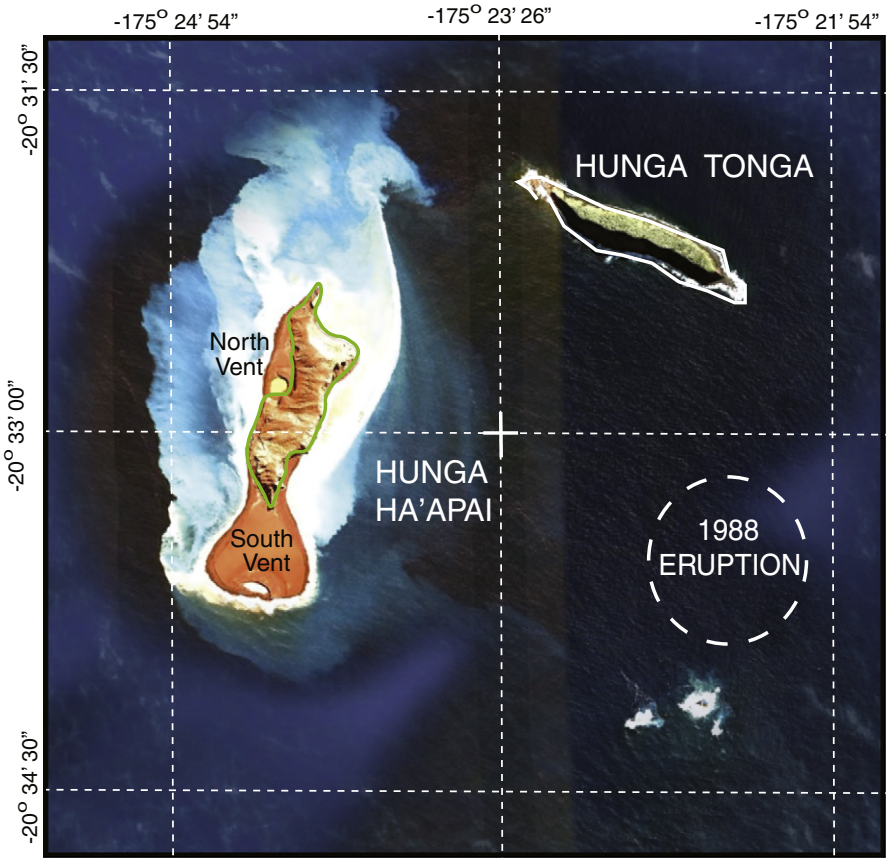

Fig. 2. Satellite image of Hunga Ha'apai and Hunga Tonga collected on 14 June 2009. Green outline shows approximate limits of Hunga Ha'apai prior to the March 2009 eruption. A white dashed line indicates the approximate location of the 1988 submarine eruption (Siebert et al., 2010; Taylor, 2010).

part of the International Monitoring System (e.g., Graeber and Piserchia, 2004; Hanson and Bowman, 2006).

3. Underwater acoustics of the March 2009 eruption

3.1. Ambient noise correlations

To evaluate long-term acoustic activity at Hunga Ha'apai-Hunga Tonga volcano, ambient noise recorded at station M3 is cross-correlated using a series of 5 s duration windows with 4 s (80%) overlap. An ambient noise "detection" is declared for any window returning Quality Level C or better results (Fig. 4a). The results prior to the March eruption are complicated by the R/V Langseth survey, which manifests itself in Fig. 4a as a series of stripes tracking the ship and airguns. Still evident in Fig. 4a, however, are a series of well-correlated detections directed at the Hunga Ha'apai island. Although the number of Hunga Ha'apai-directed detections is small, occupying only ~0.01% of the correlation windows examined prior to 17 March 2009, they define a narrow band that stands out relative to the seismic survey and background detection field (Fig. 4a). This result indicates that the volcano was acoustically active in the months prior to the eruption.

The number of well-correlated noise windows begins to increase at ~15:38 on 16 March, and the decreases sharply at ~08:50 on March 19. During this time window an average of 91% of the all cross correlation windows report detections directed from Hunga Ha'apai, and 66% of these windows correlate above the Quality Level A threshold. This constrains the primary eruptive period to be ~2.7 days in duration.

During this period, detection azimuths tend to cluster in two groups, with one peak at 95.7° and the other near 94.7° from the M3 array. Applying a correction for the ~0.30 counter-clockwise bias in the absolute azimuth, as determined from the airgun calibration (Section 2.2), the more southerly azimuth points toward the southern tip of the pre-eruptive island shoreline, and the northerly azimuth points just to the north of the island. The observed angular separation from the M3 array is slightly larger the ~0.7° difference between north and south vent sites (as observed at the sea surface). Their bimodal distribution, however, is consistent with energy coupling preferentially into the sound channel at two distinct locations along the flanks of the submerged volcanic edifice (Fig. 4b).

Initially, the recorded azimuths are aligned to the south (~95.7°), but focus toward the north (~94.7°) during the initial 6 h of activity. The detected azimuths remain focused to the north until ~15:00 on 17 March 2009 UTC, after which two detection bands are observed

Fig. 1. Regional bathymetric map and hydrophone array geometry. Red diamonds show the location of single element omni-directional hydrophones deployed near the axis of the SOFAR channel at a depth of 1000 m below the sea surface. Labels refer to mooring numbers. The red square labeled M3 shows the position of the four element horizontal array depicted in the center inset. White lines show MGL0309 cruise tracks (Dunn and Martinez, 2010). Black lines show the boundaries defining the Australian, Tongan and Niuafo'ou Plates that comprise the Lau Basin (Zellmer and Taylor, 2001). ELSC = Eastern Lau Spreading Center; CLSC = Central Lau Spreading Center; FRSC = Fonualei Rift and Spreading Center; PR = Peggy Ridge; MTJ = Mangatolu Triple Junction. The islands of the Tongan chain are shaded in black, and are identified as (A) Hunga Ha'apai and Hunga Tonga, which is the target area for our study, (B) Tongatapu, (C) Eua, (D) Kao and Tofua, (E) Ha'apai Group, (F) Vava'u, (G) Late, (H) Fonualei, (I) Niuatoputapu and Tafahi, and (K) Niuafo'ou. Marker (L) shows the location of the submarine West Mata Volcano (Resing et al., 2011). Monawai volcano (Chadwick et al., 2008; Wright et al., 2008) lies to the south of this map, near 25.9° S, 177.2° W.

simultaneously during the next 19 h. After ~12:00 on 18 March 2009 UTC, detections are again directed primarily to the south, where they remain until the detection rate declines at ~08:50 on March 19 (Fig. 4b).

Following the initial drop in detection rate, there is a secondary drop at ~18:18. At this time, a large (M_w 7.6) earthquake occurs near 23.04 °S, 174.66° W, and the acoustic energy radiated across a broad section of the Tonga Ridge from this event, and its aftershocks, temporally masks the decreasingly small amplitude signals coming from Hunga Ha'apai. Through ~10 July (JD 161), however, the average rate of detection is maintained at roughly three times the pre-eruptive rate. The detection rate declines through the remainder of July, after which the volcano enters a quiet phase that persists through the AUH recovery in April 2010 (Fig. 4a).

3.2. Initial earthquake activity

During the period 8–14 March 2009, there were six earthquakes (M 3.5–5.0) having seismically determined epicenters with ~30–100 km range of Hunga Ha'apia Island. The largest of these was felt in Nuku'alofa (International Seismological Centre, 2010). Independently locating these events using water-borne Tertiary (T-) wave arrivals detected across the Lau hydrophone array, confirms that they were positioned distant to the islands.

The acoustic record shows that the earthquake activity immediately preceding the eruption began at 15:11 UTC on 16 March 2009, approximately 14 h before the first eyewitness reports of active volcanism. This seismic event, which is not reported by land-based networks, is a precursor or foreshock to a nearly co-located m_b 4.8 earthquake that occurred 14 min later (15:25 UTC on 16 March 2009). Using Tertiary (T)-wave arrivals recorded at all six stations, both events locate near the southern tip of Hunga Ha'api, with 90% confidence ellipses that encompasses the island and western flank of the volcano (Fig. 5). The International Seismological Centre (2010) locates this event 10 km to the south–southeast of Hunga Ha'api, with the confidence ellipse that spans the southwestern flank of the volcano and abuts T-wave error ellipse.

Although the T-wave data do not provide quantitative focal depth estimates, the leading earthquake arrivals are characterized by spectral energy up to 50 Hz and the rise times of no more than 6 and 27 s for the 15:11 and 15:25 earthquakes, respectively (Fig. 5). These properties are consistent with the T-waves derived from shallow seismicity along oceanic spreading centers and transforms (cf., Yang and Forsyth, 2003; Dziak et al., 2004) and suggest that the initial Hunga Ha'apia activity is sourced at similarly shallow depths (<~10 km) within overriding Tofua Arc. By contrast, for deeper plate-interface events, which are common along the subduction zone, higher frequency energy is preferentially stripped out as the signals traverse longer solid-Earth paths through the arc crust (e.g., Salzberg, 2006), and a broader zone T-wave conversion commonly gives rise to more emergent arrivals (e.g., Talandier and Okal, 2001).

The initial T-wave energy from these leading earthquakes yields a back azimuth directed toward Hunga Ha'api. Within the T-wave coda, the dominant back azimuth rotates first to the south (increases) before swinging to the north (decreases). This tracks the reflected and backscattered energy from along the south–southwest trending arc. A similar azimuthal pattern within the coda of both T-waves is of course expected for two nearly co-located sources (Fig. 5d). These initial T-wave arrivals are followed by a handful of smaller aftershocks that occur during the next ~13 min, after which the rate and magnitude of acoustic events begin to increase in a manner inconsistent with the aftershock process (cf. Bohnenstiehl et al., 2002).

In the periods immediately prior to and between these two T-wave arrivals, cross correlation results show that the dominant ambient noise in the basin is coming from a back azimuth of 29° (Fig. 5d). This points directly toward West Mata volcano (Resing et al., 2011), which lies a distance of 640 km from the M3 array (Fig. 1). We observe West Mata to be among the most persistent sound sources during the 15-month deployment. Its frequently erupting summit behaves as point source near the axis of the sound channel, leading to a high rate of well-correlated ambient noise detections (Fig. 5d).

3.3. Evolution of the volcano-acoustic time series

As it is difficult to identify individual acoustic 'events' during much of the eruption, we instead track its intensity by examining the pressure amplitude time series (e.g., Tolstoy et al., 2006; Dziak et al., 2012). This is equivalent to the Real-time Seismic Amplitude Measurement (RSAM) approach widely used in volcano seismology (e.g., Endo and Murray, 1991). Fig. 6 shows a spectral representation of these data, overlain by the root-mean-square (rms) pressure calculated in a series of 3-min-duration windows offset by 1-min time steps. As the pressure data are omni-directional, the rate of ambient noise

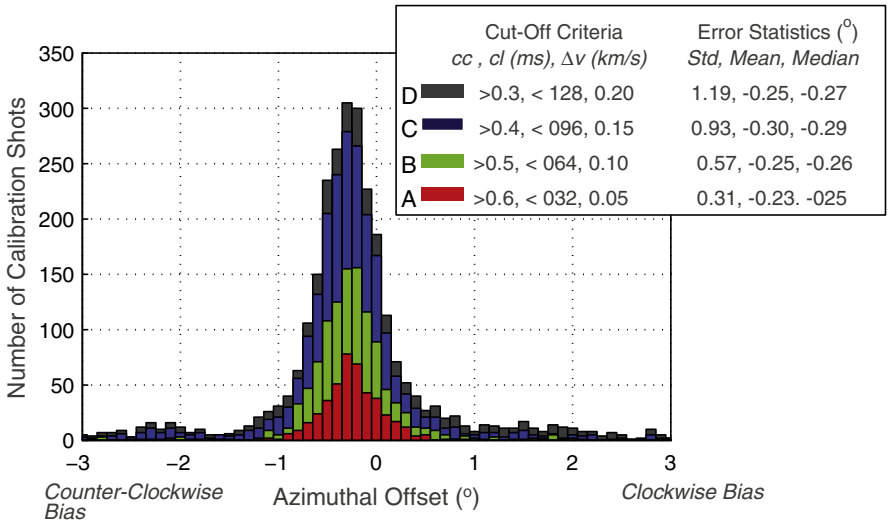

Fig. 3. Horizontal array (M3) calibration using airgun shots from cruise MGL0309 (Dunn and Martinez, 2010). Histogram depicts azimuthal difference between GPS-determined shot locations and the back-azimuth determined using the plane-wave fitting procedure. Results are filtered at various levels of data quality based on the correlation coefficient (cc), closure value (cl) and velocity (v) returned by the inversion. The standard deviation, mean and median offset are tabulated. Time lags used in the inversion were determined using 5 s duration windows band-passed between 2 and 20 Hz.

detections (Quality Level C) directed toward Hunga Ha'apai also is depicted. Fig. 7 shows a more detailed view of the rms and detection time series, and Fig. 8 shows a more detailed view of the spectral data within short time windows that track the evolution of the eruption.

Examining the initiation of activity, both the 15:11 and 15:25 earthquake events generate an increase in rms amplitude and a small number of the Hunga Ha'api directed detections (Figs. 5 and 7). A series of small earthquakes follow these events, but rms pressure levels and detection rates remain low. After ~13 min, however, T-wave signals begin to arrive at progressively shorter intervals (Fig. 8a), and there is an associated rise in rms pressure levels and azimuthal detection rates (Fig. 7). There is an additional uptick in rms pressure levels just before 16:00 h, and within a few minutes, earthquake-generated T-waves arrive in such short succession that their codas overlap (Fig. 8b). Beginning at 16:38, the low-frequency rms pressure levels increase rapidly, and detection rates rise to > 80%. Sound levels reach their peak level at 16:50 on 16 March 2009 UTC (Figs. 7 and 8c), but fall abruptly during the following 20 min.

As the rms levels decline, there is a period of sustained low-frequency (1–20 Hz) rumbling with few discrete T-wave signals (Fig. 8d). Beginning just before 19:00 on 16 March there begins a series of discrete, very-broadband arrivals that are interpreted as explosions (Fig. 8e). These transient signals are superimposed on the low frequency energy and generate a more variable rms pressure time series (Fig. 7). The variability of the rms pressure time series decreases after ~09:00 on 17 March; after which, there is an overall decline in signal amplitude during the next several days, with very-broadband signals become increasingly sparse (Figs. 7 and 8). By the afternoon of 18 March (UTC), the very-broadband signals have largely subsided and the low frequency energy continues to decline. At ~08:52 on 19 March, the detection rate drops below a few percent (Fig. 7f) as the 1–20 Hz noise levels approach background levels.

4. Volcano-acoustic inputs into the ocean soundscape

Sound plays a key role in the oceans and is used by aquatic animals for life sustaining activities such as feeding, breeding and navigation (Au and Hastings, 2008). In recent years the potential impacts of increasing anthropogenic sound on the health of individuals and ecosystems have garnered much attention (e.g., National Research Council, 2003; Soto et al., 2006; Parks et al., 2007). Natural sources of noise, however, also may play a role in modulating both the long- and short-term trends in ocean noise levels; yet, the acoustic inputs associated with submarine volcanism are poorly constrained.

To quantify the underwater acoustic energy released during the March 2009 eruption, a Range-dependent Acoustic Model (RAM) (Collins, 1993) is used to estimate the transmission loss between Hunga Ha'apai and the M3 and M4 hydrophone receivers. These two stations have the least obstructed acoustic paths from the volcano. We considered a suite of potential point source locations positioned at between 10 and 400 m in depth along the flank of the edifice downslope from both the northern and southern vents. The result predicts a minimum transmission loss of 120.0 dB rel. 1 m to the M3 array and 130.5 dB rel. 1 m to the M4 station. These values are consistent with the average range dependence identified empirically by Schiep (2012) for airgun shots propagating along the deeper-water flanks of the ELSC. Applying these minimum transmission loss values in calculating the energy flux density time series yields a minimum estimate for the acoustic energy release (see Appendix A).

The result shows that on the order of 1.7×10^{13} to 4.7×10^{13} J of acoustic energy was radiated into the water column over the 1–125 Hz band range. By comparison, the R/V Langseth survey that occurred during a 27-day period (Fig. 1) deployed a total of 9,400 airgun shots from its 36-gun acoustic array, representing on the order of 3×10^{10} J of energy. The minimum acoustic energy release by the Hunga Ha'apai eruption therefore exceeds this value by a factor of 10^3.

Hildebrand (2005, 2009) has made estimates of the annual contributions of various anthropogenic sources into the global ocean. This 10^{13} J of energy is the same order of magnitude as the total energy released annually by all seismic survey vessels (air gunning), and roughly an order of magnitude larger than the annual contribution from the global fleet of supertankers.

During the ~20 min of peak acoustic energy release, received levels at the M3 array, which lie at a distance 140 km from the volcano, are sustained in excess 150 dB_{rms} re 1 μPa. They decline afterwards, but remain above 120 dB dB_{rms} re 1 μPa over the course of the following day, throughout the period when very-broadband explosion signals are most intense. These values are well above the longer-term background level of ~90 dB re 1 μPa at M3 (Schiep, 2012), and show that the 2009 eruption of Hunga-Ha'apai-Hunga Tonga volcano may have masked low-frequency bioacoustics signals on a basin scale. Although large subduction zone earthquakes, such

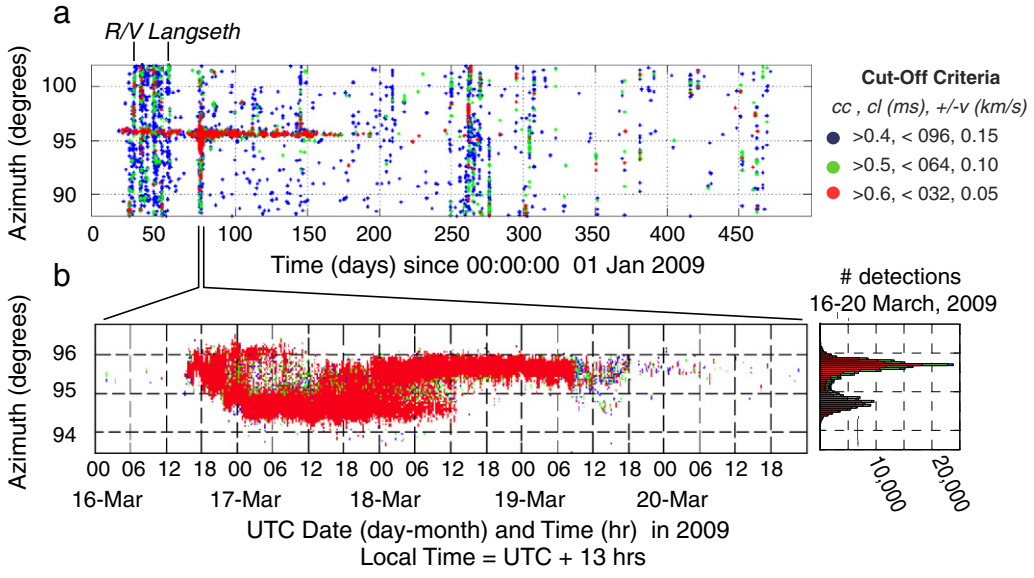

Fig. 4. a) Plot of azimuthal detection between 20 January 2009 and 15 April 2010. The results are color-coded based on the quality of the detection (see legend). b) Zoomed in view and histogram of the detections between 00:00 on 16 March and 00:00 on 21-March.

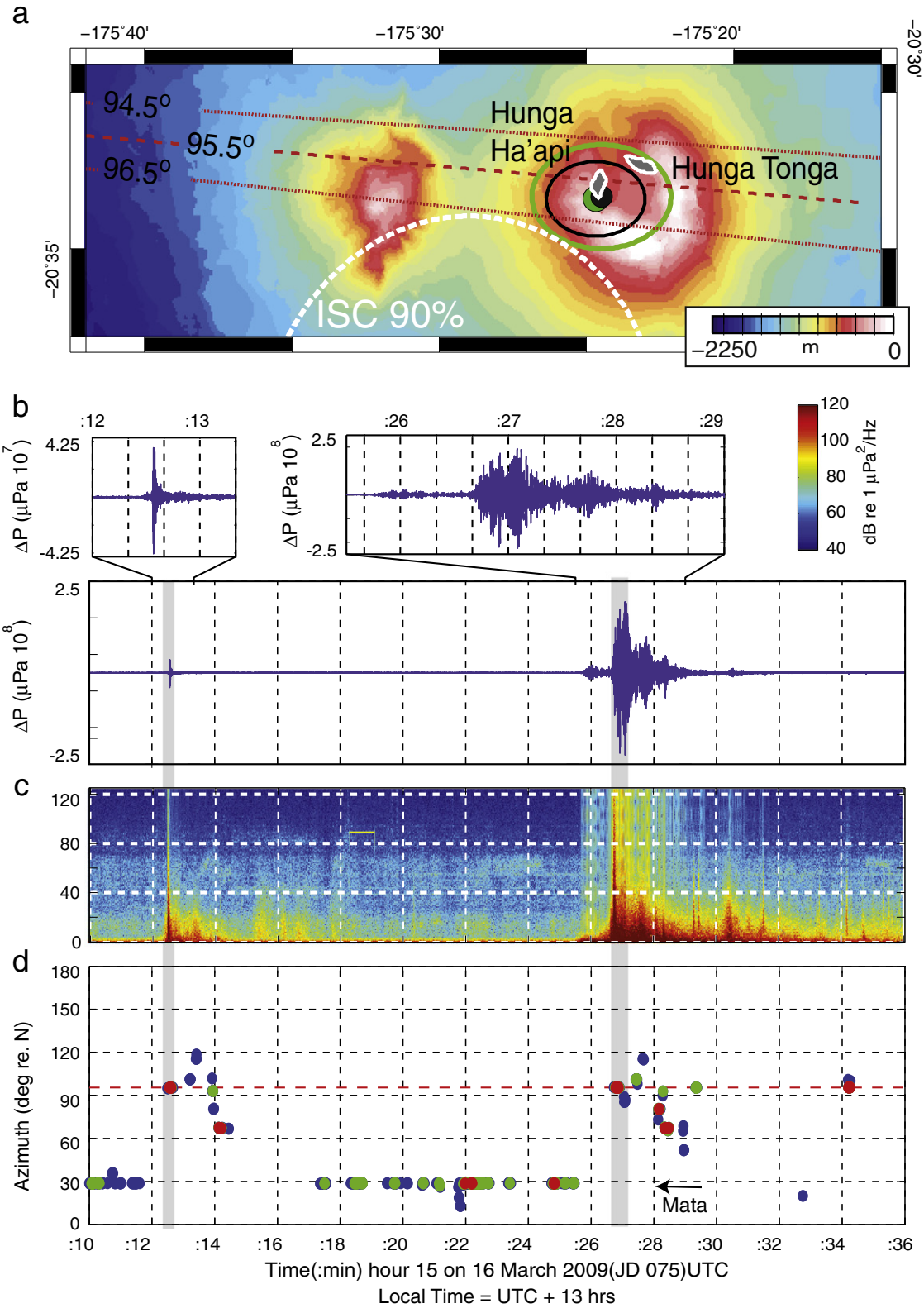

Fig. 5. a) T-wave determined locations of moderate-size earthquakes occurring during the first half of hour 15:00 on 16 March 2009. Black and green circle shows the locations, with 90% confidence, for the events originating at ~15:11 and ~15:25 UTC, respectively. The second of these events was detected teleseismically and is reported to have a body wave magnitude of 4.8 and an epicenter ~10 km southeast of Hunga-Ha'api Island. The International Seismological Centre (2010) reported 90% error ellipse (dashed with line) is shown for reference. b) Pressure waveforms showing zoomed in views of the T-wave arrivals at station M3E, ~140 km west of Hunga Ha'apai Island. c) Spectrogram of the M3E hydrophone channel. d) Back azimuth estimated from plane wave fitting routine using 5 s duration windows offset by 0.5 s (90% overlap). Data are band-passed between 2 and 20 Hz prior to performing the cross correlation. Results are sorted based on quality. Color code is the same as in Fig. 3: blue (cc > 0.4, cl < 96 ms v = 1.485 ± 0.15 km/s), green (cc > 0.5, cl < 64 ms v = 1.485 ± 0.10 km/s), red (cc > 0.6, cl < 32 ms v = 1.485 ± 0.05 km/s). Red dashed line shows a 95.5° back azimuth from station M3.

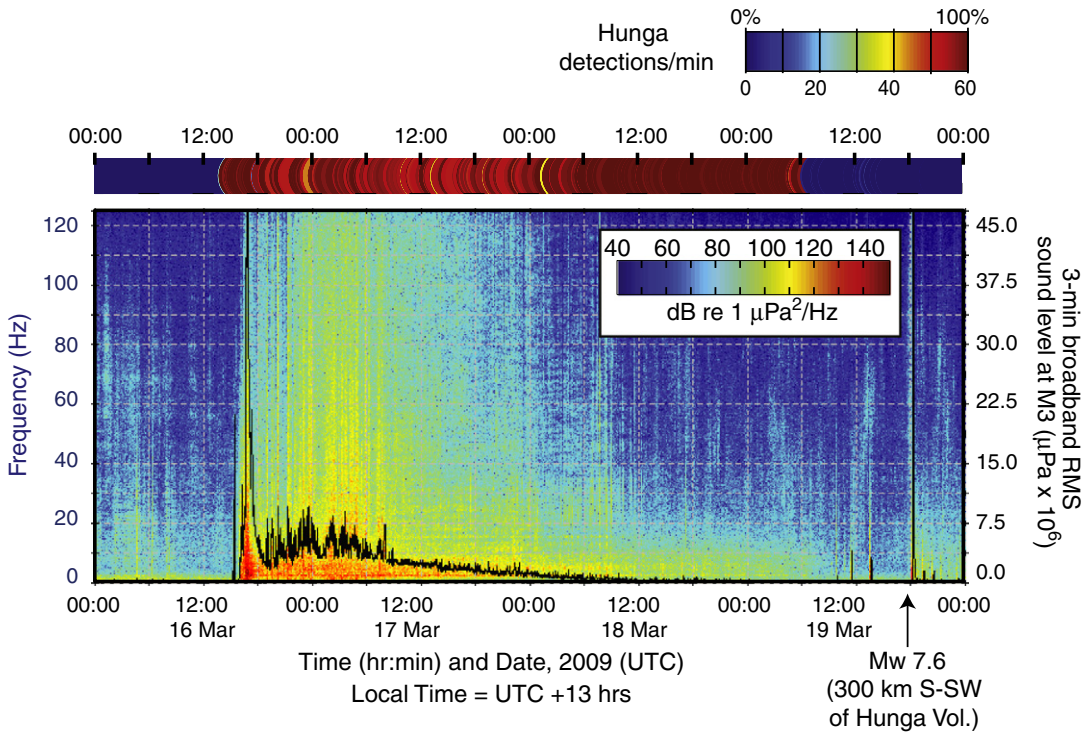

Fig. 6. Spectrogram showing the time-frequency distribution of acoustic energy recorded at station M3 between 00:00 on 16 March and 00:00 20 March 2009. The rms received sound level is overlain in black, as estimated within 3 min time windows offset in 1 min steps. Top bar shows the rate of quality level C detections with back azimuths between 93.5 and 96.5° from station M3.

as the Mw 7.6 event that occurred on 19 March 2009, are common in the area and produced even higher amplitude acoustic arrivals (Fig. 6). Their T-wave signals are sustained over much shorted (10–100 s sec) timescales (Fig. 6) and therefore may have less ecological impact.

5. Discussion

In their review of ASTER data covering the volcano, Vaughan and Webley (2010) identified a point source disturbance in the sea surface in an image collected on 12 April 2006. It was approximately 50 m wide and located ~100 m from the southern coast of the Hunga Ha'apai, near the site of the southern vent that became active during the 2009 eruption. They interpret this disturbance as a short-lived gas escape event, which was fortuitously captured within the scene. Given the sparse nature of satellite coverage and the absence of acoustic monitoring prior to January of 2009, however, it is not clear if this event is one of many, representing a long-term precursory phase of activity, or if this was merely a discrete event unrelated to the 2009 eruption. Cross-correlation analysis of the ambient acoustic time series recorded at station M3, however, shows the Hunga-Ha'apai-Hunga Ha'apai volcano to be acoustically active during a period of at least the two months prior to the March 2009 eruption (Fig. 4). Moreover, following the eruption, detection rates remain elevated through June 2009, after which the volcano enters an acoustically dormant state that persists until the array is recovered in April of 2010.

Hunga Ha'api-Hunga Tonga is in fact one of several volcanoes along the arc that intermittently generate acoustic noise during extended periods. The most persistent sources are Mata and Monoawai Volcanoes, which lie ~630 km to the north and 560 km to the south, respectively. Both are acoustically active throughout the 15-month monitoring period, and both are recognized widely as submarine volcanic systems in states of long-term (VEI ~0) eruptive activity (e.g., Chadwick et al., 2008; Wright et al., 2008; Resing et al., 2011; Watts et al., 2012). The ability of the array to track these sites of persistent eruptive activity, as wells as the more ephemeral acoustic noise leading up to and following the Hunga Ha'apai eruption, shows the potential value of including even a sparse hydrophone array as part of any effort to assess volcanic hazards within the arc.

A small-to-moderate size earthquake initiated the March 2009 activity at 15:11 on 16 March 2009 (UTC). It was followed ~14 min later by a nearly co-located magnitude 4.8 m_b earthquake. Each of these events is followed by a handful of smaller earthquakes, and the initial temporal evolution of activity appears consistent with a typical foreshock–mainshock–aftershock sequence. The spatial association of these leading earthquakes with the volcanic edifice, however, suggests that they could have been triggered in response to the inflation of the magma chamber (e.g., Thatcher and Savage, 1982; Nostro et al., 1998).

The character of the earthquake sequence changes at approximately 15:38, when the rate of earthquake activity (T-wave arrivals) begins to increase. This delay in the onset of swarm activity may suggest some feedback between the leading seismic events and the subsequent eruption. Potential mechanisms include the formation of gas bubbles in response to dynamic shaking within the magma body and static stress changes associated with fault movement. Bubble formation elevates the pressure within the chamber over time scales of ~10^3 s, until the gas percolates out of the magma (Rust and Cashman, 2004); whereas, static stress changes operate over even longer time scales, until the stress changes are ultimately relaxed by viscoelastic processes (Manga and Brodsky, 2006). Given the short delay time before the swarm is initiated (10s of minutes), both mechanisms appear viable. However, even for a moderate magnitude earthquake occurring within a few kilometers of the magma chamber, the stress change associated with either process is likely to be small (Manga and Brodsky, 2006), and consequently these potential mechanisms merely serve to advance the time of an impending eruption.

Analysis of satellite images indicates that eruption began sometime between 12:50 on 16 March, when a nighttime MODIS image

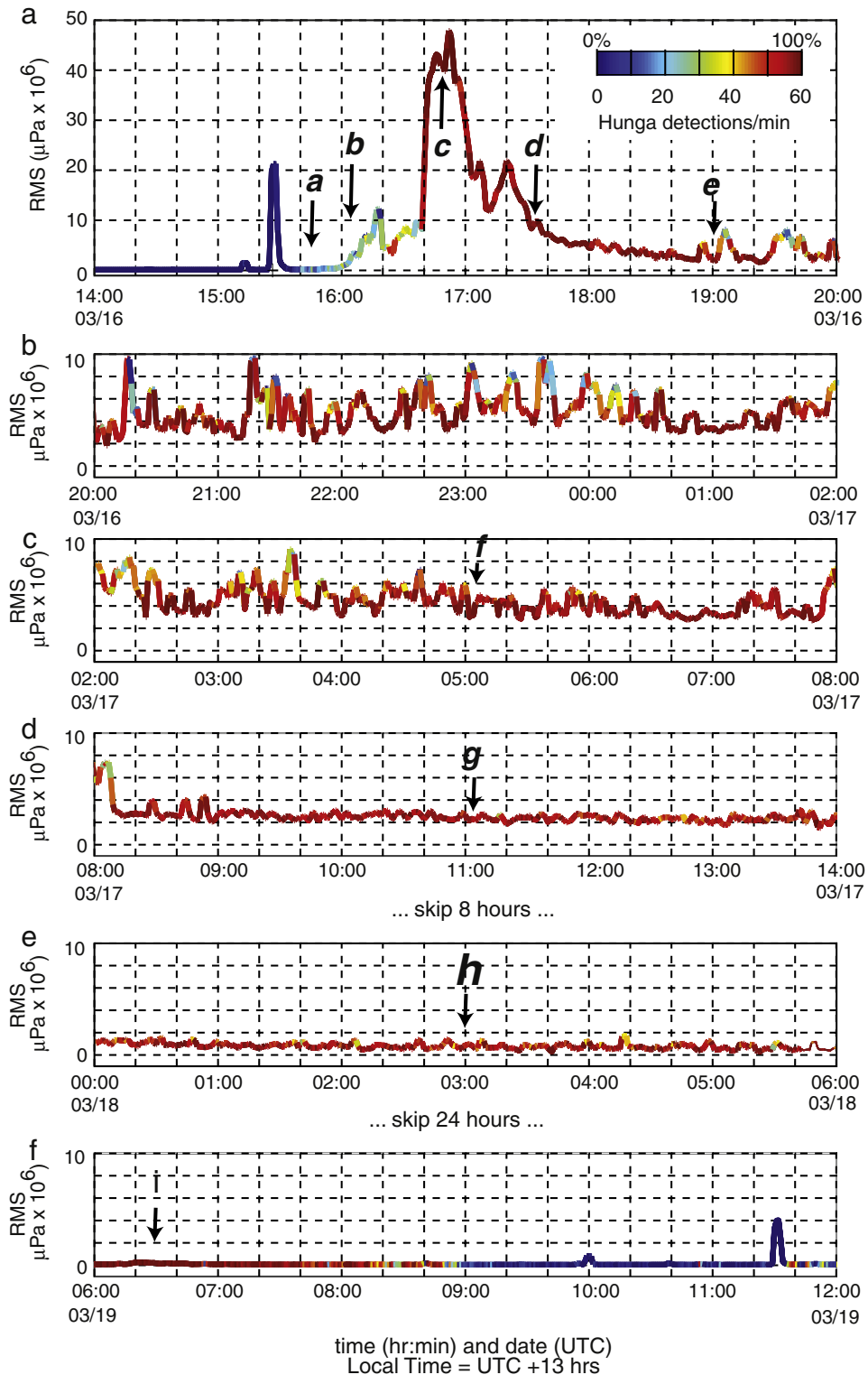

Fig. 7. Expanded view of the station M3 rms time series color-coded based on the rate of Hunga Ha'apai-directed quality level C detections. Letters refer to data examples shown in Fig. 8. Note that only panels a–d are contiguous, and that the vertical scale is expanded in panels b–f, relative to panel a.

shows no evidence of eruptive activity, and 22:10 on 16 March (UTC), when island appears to be obscured by a cloud of steam and ash (Vaughan and Webley, 2010). From the acoustic time series, this range may be narrowed considerable. The earliest seismic activity occurs at 15:11 on 16 March, but swarm activity does not initiate until 15:38 and intense swarm activity, which may mark the initial breaching of the chamber walls and movement of magma into the conduit, does not begin until ~16:00. This is followed by a sharp increase in rms amplitude and an abrupt transition toward higher (>80%) detection rates is observed at 16:40 (16 March 2009).

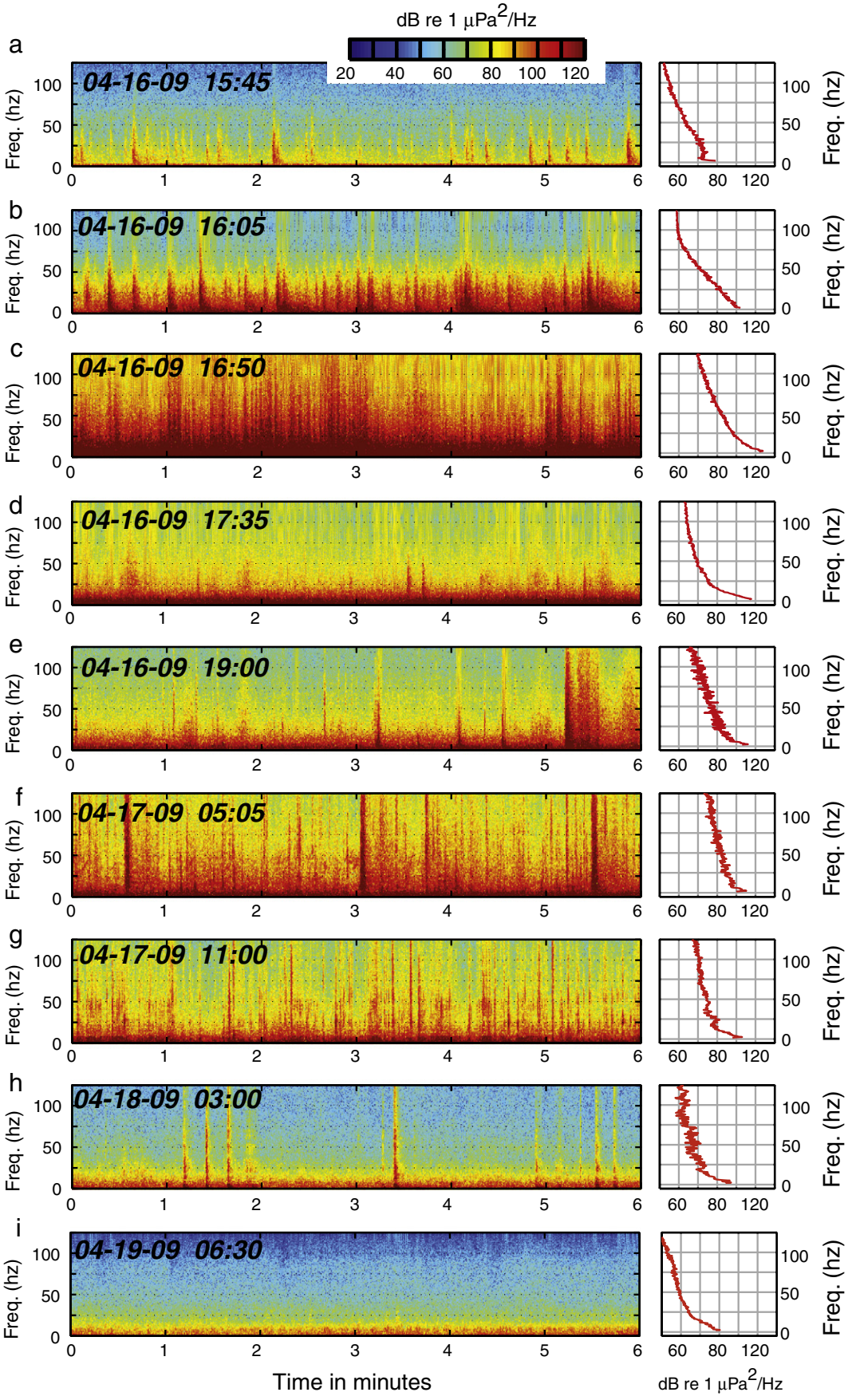

Fig. 8. Spectrograms showing data examples throughout the March 2009 eruptive event at Hunga Ha'apai-Hunga Tonga volcano. Panels on the right show the average spectra for each 6 min duration data window. Time stamp indicates the start time (UTC) of each window. See text for discussion.

Notably, changes in detection rate at M3 are not merely a function of received level. Shallow crustal earthquake can produce high signal-to-noise arrivals; yet, as evident from the initial T-wave signals (Fig. 5), the detection rates can be low and the azimuth may vary as a function of time throughout the T-wave coda. This reflects the fact that the T-wave packet is the summation of energy scatter at the seafloor interface above the earthquake hypocenter — with deeper events scattering energy over larger areas (e.g., Schreiner et al., 1995; Slack et al., 1999), producing less coherent arrivals at the quad array. By comparison, weaker sources originating from the shallow, sound-channel-breaching summit of West Mata Volcano (~1200 mbsl) often produce higher detection rates and a more consistent range of azimuths (Fig. 5d). Consequently, the transition in detection rate is interpreted to track the migration of acoustic sources into the shallow conduit.

The rms pressure time series shows a short duration (<1 h) period of intense underwater acoustic energy release that occurs within the first two hours of the eruptive sequence (Figs. 6 and 7). This pattern is similar to submarine eruptions record by in situ ocean bottom sensors along the East Pacific Rise (Tolstoy et al., 2006) and Axial Volcano on the Juan de Fuca Ridge (Dziak et al., 2012). In both cases, brief periods of high rms pressure or ground displacement have been interpreted to track the rise of the dike from the magma chamber through the brittle fracturing of the overlying oceanic crust. Similarly, for the Hunga-Ha'apai-Hunga Tonga eruption, this period is interpreted to delineate the opening or clearing of the volcanic conduit.

Once the conduit opens, brittle cracking and its associated acoustic energy release decline, and a continuous low-frequency signal can be observed to dominate the spectra (Figs. 6 and 8). Whereas narrow band tremor, associated with resonance or repeating event behavior, has been widely reported in seismic and acoustic studies of subaerial (e.g., Johnson and Lees, 2000; McNutt and Nishimura, 2008) and submarine (e.g., Dziak and Fox, 2002) volcanoes; this signal is wide band (1–20 Hz) and continues for more than 2.5 days. It generates a coherent arrival at the M3 array, suggesting a shallow source, possibly associated with the motion of the conduit walls, as magma is transported upwards, and/or material is erupted onto the seafloor.

By 19:00 on 16 March, as the wide-band low-frequency signal persists, a series of transient very-broadband (1–125 Hz) signals begin to arrive. These events are differentiated from earlier T-wave swarm activity by both their higher frequency content (>50 Hz) and more impulse character. This style of activity is sustained through 22:10 on 16 March (UTC), when confirmation of the eruption is obtained using MODIS imagery (Vaughan and Webley, 2010), and it persists during the next two days when eyewitness observations from air (first at 05:05 UTC on 17 March), land and sea report explosive activity. These very-broadband signals are interpreted to represent individual surtseyan explosive events.

After ~09:00 on 17 March, the rms pressure time series shows a transition toward less short-term variability and a gradual declining amplitude (Fig. 7). Through time the maximum amplitudes of the transient explosions decrease as the repose time between the events increases (Fig. 8). By the afternoon of 18 March (UTC), these transient signals become increasingly rare; but low-frequency signal persists and the M3-detection rate remains high (>80%). The detection rate drops suddenly just before 09:00 on 19 March 2009, as the low frequency noise continues to decline. Although small steam event are likely during the following days (Vaughan and Webley, 2010), this is interpreted to mark end of the main eruptive event.

Back azimuth calculations show two azimuthal peaks that vary temporally throughout the eruption sequence (Fig. 4). However, the initial transition in azimuths from the south to the north begins after the surtseyan phase of the eruption is initiated, and changes in the dominant azimuth direction are not clearly associated with distinct changes in the acoustic signature. Ground and satellite-based observations are too intermittent to verify a shift in activity throughout the course of the eruption. However, eyewitness reports indicate that both vent sites where active during the morning of 18 March UTC (afternoon LT), with the southern vent producing more spectacular eruptions (Taylor, 2010). This is near the tail end of the overlap period when both acoustic source regions appear active simultaneously, with the greater number of detections originating from the south (Fig. 4b).

6. Summary

Underwater acoustic recordings from a regional hydrophone array are used to track the progression of seismo-acoustic and eruptive active at Hunga Ha'apai-Hunga Tonga volcano. The acoustic signals define several phases of activity that summarize the sequence of events surrounding the March 2009 eruption.

Phase 1 (prior to 16 March, 2009): From the beginning of the deployment in January of 2009, the volcano generates low-level acoustic noise that can be identified by correlation analysis using a four-element horizontal hydrophone array (M3) at a range of ~140 km from the volcano. While the rate of detection is low, this shows the volcano to be in an acoustically active state during the months prior to the eruption.

Phase 2 (15:11–15:38 UTC, 16 March): Seismic activity immediately preceded the eruption of Hunga Ha'apai-Hunga Tonga volcano begins at 15:11 UTC on 16 March. This event is a foreshock to a nearly co-located m_b 4.8 earthquake that occurs some 14 min later (15:25 UTC on 16 March 2009). A few smaller aftershocks follow both events.

Phase 3 (15:38–16:38 UTC, 16 March): Beginning at 15:38, the rate of earthquake activity begins to increase in a manner that is inconsistent with the aftershock process. A succession of small amplitude T-waves arrive at progressively shorter intervals, until individual events can no longer be defined.

Phase 4 (16:38–~17:10 UTC, 16 March): Beginning at 16:38, the rms pressure levels increase by a factor of five, and the signal becomes more coherent, with >80% of the M3 correlation windows reporting Hunga-Ha'apai directed detections. Acoustic pressure reaches its peak value at ~16:50 and then drops rapidly in amplitude during the following 20 min. This period is interpreted to mark an intense period of brittle fracturing associated with the establishment of the shallow volcanic conduit.

Phase 5 (~17:10–18:50 UTC, 16 March): As sound levels decline, the acoustic signature of the volcano is dominated by a wide-band low-frequency (1–20 Hz) signal with few discrete events. The origin of the signal is unclear, but it is well correlated across the M3 array, suggesting a shallow source, perhaps associated with the movement of magma in the shallow conduit or the extrusion of material onto the seafloor. This wide-band signal persists through the morning of 19 March.

Phase 6 (18:50 UTC, 16 March–09:00 UTC, 17 March): Around 18:50 on 16 March, surtseyan-style explosive activity is initiated and a series of very-broadband (1–125 Hz) transient acoustic signals arrive superimposed on low frequency wide-band noise. This phase is delineated by a period of more variable rms amplitude (Figs. 6 and 7) that arises due to variability in the amplitude and clustering of these explosions.

Phase 7 (09:00 UTC, 17 March–08:52 UTC, 19 March): At ~09:00 on 17 March, there is a notable decrease in the rms pressure variability, which is sustained during the following two days. This is associated with a decrease in the intensity of the explosive activity. As the acoustic levels continue to decrease, explosive activity fades and at approximately 08:52 on 19 March the low frequency

(1–20 Hz) noise drops to background levels and the rate of detection at the M3 array drops suddenly.

Phase 8 (08:52 UTC, 19 March–June 2009): After the main eruption ends, steam driven activity continues for as a much as a few weeks (Vaughan and Webley, 2010). During the next three months the volcano continues to be a source of ambient noise, with detection rates that are elevated slightly relative to the pre-eruptive period. By July 2009, the volcano enters an acoustically dormant state, which persists until the array is recovered in April of 2010.

Although Hunga Ha'apai-Hunga Tonga volcano can be identified as an acoustically active source during the months leading up to its eruption, the volcano provided little short-term warning prior to its eruption in March of 2009. The volcanic conduit appears to have opened rapidly, within two hours of the initial seismic activity and explosive volcanism commenced soon after, within four hours of the first seismic activity.

The eruption duration is constrained to be on the order of 2.7 days, during which time the low-frequency acoustic energy input into the ocean is on the order of 10^{13} J. This value rivals the global annual acoustic inputs associated with seismic surveying and supertanker shipping — two much publicized anthropogenic sources. Yet, the degree to which marine organisms respond, or have become habituated, to volcano-acoustic events like the March 2009 eruption of Hunga-Ha'apai-Hunga Tonga volcano is unknown.

Acknowledgments

We thank the captain and crew of the R/V Marcus G. Langseth, R/V Roger Revelle and R/V Kilo Moana. Critical to the success of this project were NOAA field technicians J. Shanley and M. Fowler, who oversaw the mooring deployment and recovery efforts, and NCSU graduate students J. Bowman, K. Cook, P. Monigle, J. O'Connor, C. Scheip, and K. Warren. The manuscript was improved based on the detailed comments provided by Dr. Won Sang Lee and an anonymous reviewer; their efforts are gratefully acknowledged. This is NOAA-PMEL contribution # 3892. The work was supported by the National Science Foundation grants OCE-0825295 and OCE-1029278.

Appendix A. Underwater acoustic energy calculations

The underwater acoustic energy radiated during the March 2009 eruption of Hunga-Ha'apai-Hunga Tonga Volcano is calculated over the 1–125 Hz band following the procedures outlined by Hildebrand (2005, 2009). From first principles, the source level pressure (referenced to a range of 1 m) is converted to acoustic intensity (I) by dividing the squared pressure (p) by acoustic impedance (ρc),

$$I = \frac{p^2}{\rho c} \quad \left(\text{in units of } W/m^2\right)$$

where ρ is the density of the medium (1030 kg/m^3) and c the sound speed (1485 m/s). The acoustic power (P) is then given by the product of the intensity and a geometric factor, which is taken to be 2π (m^2) for a near surface source radiating into a half-space.

$$P = 2\pi * I(\text{in units of } W = J/s)$$

Acoustic energy is then calculated as the linear product of the signal power and duration (T).

$$E = P * T(\text{in units of } J)$$

This calculation is applied to a series of non-overlapping 1 s duration windows that span the time period between 15:00 UTC on 16 March 2009 and 09:00 UTC on 19 March 2009. After the energy contribution from the background acoustic field is removed (e.g., Holt et al., 2009), the results are summed to estimate the total amount of acoustic energy released during the eruption. The procedure is carried out independently for stations M3 and M4, which are the station that lie along the least obstructed acoustic paths from the volcano. The results yield estimates of 1.7×10^{13} and 4.7×10^{13} J for the two respective stations.

References

Au, W.W., Hastings, M.C., 2008. Principles of Marine Bioacoustics. Springer, p. 695.
Bohnenstiehl, D.R., Tolstoy, M., Dziak, R.P., Fox, C.G., Smith, D.K., 2002. Aftershock sequences in the mid-ocean ridge environment: an analysis using hydroacoustic data. Tectonophysics 354, 49–70.
Bryan, W.B., Stice, G.D., Ewart, A., 1972. Geology, petrography, and geochemistry of the volcanic islands of Tonga. Journal of Geophysical Research 77, 1566–1585.
Chadwick Jr., W.W., Wright, I.C., Schwarz-Schampera, U., Hyvernaud, O., Reymond, D., de Ronde, C.E.J., 2008. Cyclic eruptions and sector collapses at Monowai submarine volcano, Kermadec arc: 1998–2007. Geochemistry, Geophysics, Geosystems 9, Q10014 http://dx.doi.org/10.1029/2008GC002113.
Chapp, E., Bohnenstiehl, D.R., Tolstoy, M., 2005. Sound-channel observations of ice-generated tremor in the Indian Ocean. Geochemistry, Geophysics, Geosystems 6, Q06003 http://dx.doi.org/10.1029/2004GC000889.
Collins, M.D., 1993. A split-step Pade solution for the parabolic equation method. Journal of the Acoustical Society of America 93, 1736–1742.
de Groot-Hedlin, C., Orcutt, J., 2001. Excitation of T-phases by seafloor scattering. Journal of the Acoustical Society of America 109, 1944–1954.
Del Pezzo, E., Giudicepietro, F., 2002. Plane-wave fitting method for a plane, small aperture, short period seismic array: a MATHCAD program. Computers & Geosciences 28, 59–64.
Dunn, R.A., Martinez, F., 2010. Contrasting crustal production and rapid mantle transitions beneath back-arc ridges. Nature 46, 198–202 http://dx.doi.org/10.1038/nature09690.
Dziak, R.P., Fox, C.G., 2002. Evidence of harmonic tremor from a submarine volcano detected across the Pacific Ocean basin. Journal of Geophysical Research 107 http://dx.doi.org/10.1029/2001JB000177.
Dziak, R.P., Smith, D.K., Bohnenstiehl, D.R., Fox, C.G., Desbruyeres, D., Matsumoto, H., Tolstoy, M., Fornari, D.J., 2004. Evidence of a recent magma dike intrusion at the slow spreading Lucky Strike segment, Mid-Atlantic Ridge. Journal of Geophysical Research 109 http://dx.doi.org/10.1029/2004JB003141.
Dziak, R.P., Haxel, J.H., Bohnenstiehl, D.R., Chadwick Jr., W.W., Nooner, S.L., Fowler, M.J., Matsumoto, H., 2012. Seismic precursors and magma ascent before the April 2011 eruption at Axial Seamount. Nature Geoscience 5, 1–5 http://dx.doi.org/10.1038/ngeo1490.
Endo, E.T., Murray, T., 1991. Real-time seismic amplitude measurement (RSAM): a volcano monitoring and prediction tool. Bulletin of Volcanology 53, 533–545.
Fox, C., Matsumoto, H., Lau, T.-K., 2001. Monitoring Pacific Ocean seismicity from an autonomous hydrophone array. Journal of Geophysical Research 106, 4183–4206.
Graeber, F.M., Piserchia, P.-F., 2004. Zones of T-wave excitation in the NE Indian ocean mapped using variations in backazimuth over time obtained from multi-channel correlation of IMS hydrophone triplet data. Geophysical Journal International 158, 239–256 http://dx.doi.org/10.1111/j.1365-246X.2004.02301.x.
Hanson, J.A., Bowman, J.R., 2006. Methods for monitoring hydroacoustic events using direct and reflected T-waves in the Indian Ocean. Journal of Geophysical Research 111 http://dx.doi.org/10.1029/2004JB003609.
Hildebrand, J.A., 2005. Impacts of anthropogenic sound. In: Reynolds III, J.E., Perrin, W.F., Reeves, R.R., Montgomery, S., Ragen, T.J. (Eds.), Marine Mammal Research: Conservation Beyond Crisis. The Johns Hopkins University Press, Baltimore, Maryland, pp. 101–124.
Hildebrand, J., 2009. Anthropogenic and natural sources of ambient noise in the ocean. Marine Ecology Progress Series 395, 5–20 http://dx.doi.org/10.3354/meps08353.
Holt, M.M., Noren, D.P., Veirs, V., Emmons, C.K., Veirs, S., 2009. Speaking up: killer whales (*Orcinus orca*) increase their call amplitude in response to vessel noise. Journal of the Acoustical Society of America 125, EL27 http://dx.doi.org/10.1121/1.3040028.
International Seismological Centre, 2010. On-line Bulletin. http://www.isc.ac.uk Internatl. Seis. Cent., Thatcham, United Kingdom.
Johnson, J., Lees, J., 2000. Plugs and chugs — seismic and acoustic observations of degassing explosions at Karymsky, Russia and Sangay, Ecuador. Journal of Volcanology and Geothermal Research 101, 67–82.
Manga, M., Brodsky, E., 2006. Seismic triggering of eruptions in the far field: volcanoes and geysers. Annual Review of Earth and Planetary Sciences 34, 263–291.
McNutt, S.R., Nishimura, T., 2008. Volcanic tremor during eruptions: temporal characteristics, scaling and constraints on conduit size and processes. Journal of Volcanology and Geothermal Research 178, 12–20 http://dx.doi.org/10.1016/j.jvolgeores.2008.03.010.
National Research Council, 2003. Ocean Noise and Marine Mammals. National Academies Press, Washington DC, p. 208.
Nostro, C., Stein, R.S., Cocco, M., Belardinelli, M.E., Marzocchi, W., 1998. Two-way coupling between Vesuvius eruptions and southern Apennine earthquakes (Italy) by elastic stress transfer. Journal of Geophysical Research 103, 24,487–24,504.
Parks, S.E., Clark, C.W., Tyack, P.L., 2007. Short- and long-term changes in right whale calling behavior: the potential effects of noise on acoustic communication. Journal of the Acoustical Society of America 122, 3725–3731 http://dx.doi.org/10.1121/1.2799904.

Parson, L.M., Hawkins, J.W., 1994. Two-stage ridge propagating and the geological history of the Lau backarc basin. Proceeding of the Ocean Drilling Program, Scientific Results 135, 819–828.
Parson, L.M., Wright, I.C., 1996. The Lau-Havre-Taupo back-arc basin: a southward propagating, multi-stage evolution from rifting to spreading. Tectonophysics 263, 1–22.
Resing, J.A., Rubin, K.H., Embley, R.W., Lupton, J.E., Baker, E.T., Dziak, R.P., Baumberger, T., et al., 2011. Active submarine eruption of boninite in the northeastern Lau Basin. Nature Geoscience 4, 799–806 http://dx.doi.org/10.1038/ngeo1275.
Rust, A.C., Cashman, K.V., 2004. Permeability of vesicular silicic magma: inertial and hysteresis effects. Earth and Planetary Science Letters 228, 93–107.
Salzberg, D., 2006. Using T-phase spectra to estimate rupture depth and static offset of the seafloor. Journal of the Acoustical Society of America 119, 3252-3252.
Schiep, C.M., 2012. Acoustic Variability of a Seismic Airgun Survey in the Lau Back-Arc Basin, M.S. Thesis, North Carolina State University.
Schreiner, A.E., Fox, C.G., Dziak, R.P., 1995. Spectra and magnitudes of T-waves from the 1993 earthquake swarm on the Juan de Fuca Ridge. Geophysical Research Letters 22, 139–142.
Siebert, L., Simkin, T., Kimberly, P., 2010. Volcanoes of the World, 3rd edition. Smithsonian Institution, p. 551.
Slack, P.D., Fox, C.G., Dziak, R.P., 1999. P wave detection thresholds, Pn velocity estimates, and T wave location uncertainty from oceanic hydrophones. Journal of Geophysical Research 104, 13,061–13,072 http://dx.doi.org/10.1029/1999JB900112.
Smithsonian Institution, 2009. Hunga Tonga-Hunga Ha'apai. Bulletin of the Global Volcanism Network (BGVN) 34 (03).
Soto, N.A., Johnson, M., Madsen, P.T., Tyack, P.L., Bocconcelli, A., Borsan, J.F., 2006. Does intense ship noise disrupt foraging in deep-diving Cuvier's beaked whales (*Ziphius Cavirostris*)? Marine Mammal Science 22, 690–699 http://dx.doi.org/10.1111/j.1748-7692.2006.00044.x.
Talandier, J., Okal, E., 2001. Identification criteria for sources of T waves recorded in French Polynesia. Pure and Applied Geophysics 158, 567–603.
Taylor, P., 2010. The March 2009 eruption of the Hunga Tonga and Hunga Ha'apai Volcano, Kingdom of Tonga. SOPAC Report 717b, abstract 2010–46.
Taylor, B., Zellmer, K., Martinez, F., Goodliffe, A., 1996. Sea-floor spreading in the Lau back-arc basin. Earth and Planetary Science Letters 144, 35–40.
Thatcher, W., Savage, J.C., 1982. Triggering of large earthquakes by magma-chamber inflation, Izu Peninsula, Japan. Geology 10, 637–640.
Tolstoy, M., Cowen, J.P., Baker, E.T., Fornari, D.J., Rubin, K.H., Shank, T.M., Waldhauser, F., Bohnenstiehl, D.R., Forsyth, D.W., Holmes, R.C., Love, B., Perfit, M.R., Weekly, R.T., Soule, S.A., Glazer, B., 2006. A seafloor spreading event captured by seismometers. Science 314, 1920–1922 http://dx.doi.org/10.1126/science.1133950.
Vaughan, R.G., Webley, P.W., 2010. Satellite observations of a surtseyan eruption: Hunga Ha'apai, Tonga. Journal of Volcanology and Geothermal Research 198, 177–186 http://dx.doi.org/10.1016/j.jvolgeores.2010.08.017.
Watts, A.B., Peirce, C., Grevemeyer, I., Paulatto, M., Stratford, W., Bassett, D., Hunter, J.A., et al., 2012. Rapid rates of growth and collapse of Monowai submarine volcano in the Kermadec Arc. Nature Geoscience 5 http://dx.doi.org/10.1038/ngeo1473.
Wright, I.C., Chadwick, W.W., de Ronde, C.E.J., Reymond, D., Hyvernaud, O., Gennerich, H.H., Stoffers, P., Mackay, K., Dunkin, M.A., Bannister, S.C., 2008. Collapse and reconstruction of Monowai submarine volcano, Kermadec arc, 1998–2004. Journal of Geophysical Research 113, 1–13.
Yang, Y., Forsyth, D.W., 2003. Improving epicentral and magnitude estimation of earthquakes from T phases by considering the excitation function. Bulletin of the Seismological Society of America 93, 2106–2122.
Zellmer, K., Taylor, B., 2001. A three-plate kinematic model for Lau Basin opening. Geochemistry, Geophysics, Geosystems 2 http://dx.doi.org/10.1029/2000GC000106.